# Internal Strain Measurements and X-ray Imaging in Interpenetrating-Phase $Al_2O_3$/Al Composites

Marcus L. Young[1,2], Jon D. Almer[2], Ulrich Lienert[2], Kamel Fezzaa[2], Wah-Keat Lee[2], Dean R. Haeffner[2], and David C. Dunand[1]

[1] Northwestern University, Evanston, IL, U.S.A.; [2] Argonne National Laboratory, Argonne, IL, U.S.A.

## Introduction

Interpenetrating phase composites (IPCs) are characterized by two co-continuous and percolating phases. Ceramic-metal IPCs typically exhibit much higher toughness than pure ceramics, e.g., cermets such as WC-Co with high-metal content. Several liquid-metal processing routes exist for creating $Al_2O_3$-Al IPCs, including infiltration of porous $Al_2O_3$ preforms [1], reactive metal penetration [2], and displacement reactions [3]. Ceramic-metal IPCs with a highly regular architecture and tailored properties can be fabricated from a number of techniques involving solid freeform ceramic preforms with complex three-dimensional (3-D) ceramic architectures. One direct-write technique, known as robocasting, can be used to create the aforementioned preforms by extruding colloidal inks in a layer-wise fashion [4-6]. Here, we study the mechanical properties of such an $Al_2O_3$-Al IPC.

## Methods and Materials

As described in more detail previously [7, 8], $Al_2O_3$ preforms with a regular 0/90 architecture were produced by robotic deposition using a gel-based ink (with 5 vol% $ZrO_2$ as sintering aid). The first layer is composed of a series of equidistant rods (250 μm in diameter) parallel to the x-axis with "hairpins" connecting them. The second layer is identical to the first but rotated by 90 degrees, i.e., is parallel to the y-axis. This process was repeated 15 times, resulting in a 30-layer preform with simple-cubic symmetry. Alternatively, by offsetting the every other layer by one rod diameter, a face-centered-cubic symmetry preform was created. Sintered $Al_2O_3$ preforms were gas-pressure, liquid-metal infiltrated with either 99.99% pure aluminum or aluminum alloy 7075, as described in detail previously [8, 9]. The resulting composites were machined to 5.2x5.2x9.9 $mm^3$ parallelepipeds with the ceramic preform remaining completely incased within aluminum. The pure aluminum matrix composites were annealed for 2 h at 350°C and air cooled prior to compression testing. The aluminum alloy 7075 matrix composites were subsequently annealed for 1 hour at 490°C, water quenched, annealed for 24 hours at 120°C, and then water quenched again.

High-energy, phase-contrast x-ray imaging was performed at the 1-ID beam line of the Advanced Photon Source (Argonne National Laboratory). Ceramic preforms and pre- and post-compression testing composites of both symmetries were imaged. The samples were positioned with their vertical faces perpendicular/parallel (0/90°) to the beam. Radiographic images were collected using a monochromatic 81 keV (λ= 0.015 nm) x-ray beam with a square cross-sectional field of view of 2x2 $mm^2$. Images were recorded using a CCD camera, positioned far enough from the sample to allow for phase propagation (phase-enhanced imaging) [10].

High-energy x-ray diffraction measurements were made at the 1-ID and 11-ID beam lines of the Advanced Photon Source. *In-situ* uniaxial compressive testing was performed using a small, custom-built, screw-driven loading system. The general setup for these experiments has been described in detail previously [8, 11].

Two face-centered-cubic symmetry composites were subjected to uniaxial compressive loading with ca. 15 MPa stress increments. At each stress level, diffraction measurements were performed with a monochromatic 81 or 93 keV (λ= 0.015 or 0.013 nm) x-ray beam for 20 to 60 seconds. The x-ray beam generally had a square cross-section with a size of 150 x 150 $\mu m^2$. The sample-to-camera distance was 1.22 or 2.10 m. The samples were positioned either for spatially-resolved measurements with their vertical faces perpendicular/parallel (0/90°) to the beam or for average bulk measurements with the faces at a 22° angle. For spatially-resolved measurements, the beam was positioned perpendicular to the center of the sample. Since the beam width (150 μm) is smaller than the $Al_2O_3$ strut width (ca. 250 μm), the beam path was within one of the horizontal rods, which consist of roughly equal fractions of columns and struts. For the average bulk measurements, strain measurements were collected during a vertical 3 mm raster near the middle of the sample. Determination of lattice strains from the diffracted rings recorded by the camera has been previously described in detail [8].

### RESULTS & DISCUSSION

As seen in Figure 1a and 1b, x-ray images of the ceramic preform illustrate the layering difference between face-centered-cubic and the simple-cubic symmetry.

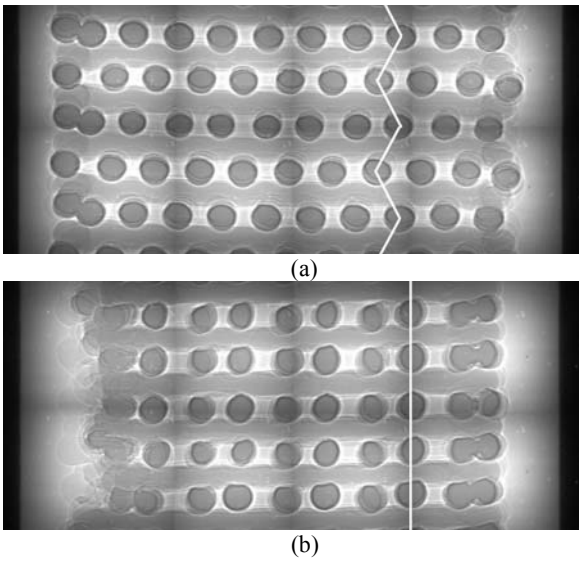

(a)

(b)

Figure 1. X-ray phase-enhanced images of (a) a face-centered-cubic symmetry and (b) a simple-cubic symmetry. The rod diameter is 250 $\mu$m. The white line was added to highlight the layering difference between the two preforms.

X-ray phase-enhanced images of a face-centered-cubic symmetry composite and a simple-cubic symmetry composite after being tested in compression to failure, which occurred at 250 and 300 MPa, respectively, are shown in Figure 2a and b. Fracture of the ceramic preform within the composite can be seen as a combination of vertical and angular cracks occurring along the span underneath the previous horizontal rod for the face-centered-cubic symmetry composites and as mostly vertical cracks for the simple-cubic symmetry composites. For both symmetries, fracture occurred predominately near the edges of the sample where the aluminum is less constrained leading to alumina damage and displacement.

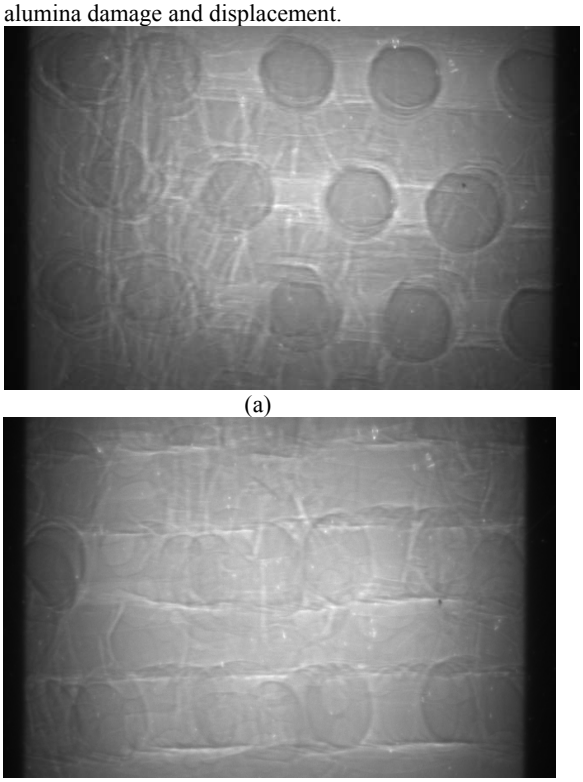

(a)

(b)

Figure 2. An x-ray phase-enhanced images illustrating typical crack behavior for composites with (a) face-centered-cubic symmetry and (b) simple-cubic symmetry.

X-ray diffraction rings for the Al phase were incomplete, due to the large grain size of aluminum (due to the casting method) as compared to the irradiated volume. Thus no strain was measured for the matrix. The $Al_2O_3$ and $ZrO_2$ phases exhibited complete rings, as expected from the fine grain size of the alumina and zirconia processed as described previously [8]. Previous spatially-resolved strain measurements during compression were reported on two samples with similar properties to the samples discussed here [8].

A face-centered-cubic symmetry sample, with a density of 3.41 g/cm$^3$ (corresponding to an Al alloy 7075 volume fraction of 44.1%), was cyclically tested without failure as follows: 0 → 85 → 50 MPa, 50 → 165 → 50 MPa, and 50 → 325 → 0 MPa. Plots of the applied stress vs. average elastic lattice strain were created for several $Al_2O_3$ and $ZrO_2$ (hkl) planes. One such plot for the $Al_2O_3$ (113) plane, which is representative of typical $Al_2O_3$ (hkl) planes, is presented in Figure 3a.

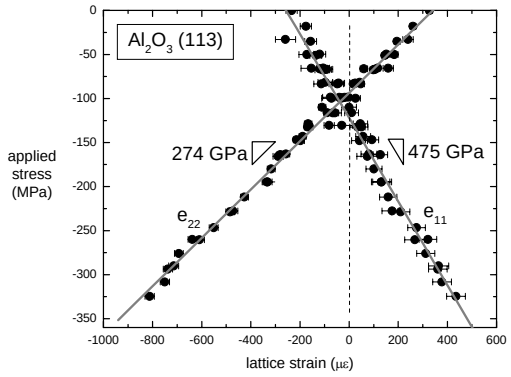


(a)

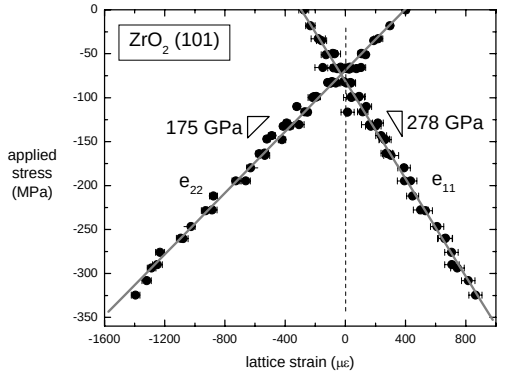


(b)

Figure 3. Applied stress vs. lattice strain for an Al/$Al_2O_3$ composite with face-centered-cubic symmetry, using (a) $Al_2O_3$ (113) and (b) $ZrO_2$ (101) reflections, upon cyclical loading. The strains $e_{11}$ and $e_{22}$ are perpendicular and parallel to the direction of the applied stress, respectively.

Upon cyclical elastic loading, the apparent elastic modulus of the alumina phase ($E_{app}$=275 GPa, defined as the applied stress divided by average lattice strain $e_{22}$ in the same direction as the applied stress) was lower than the elastic modulus of pure $Al_2O_3$ (E=410 GPa). This is a result of load transfer from the aluminum to the alumina phase and indicates that the stress carried by the alumina phase is higher than the applied stress, as observed in many other metal-ceramic systems e.g. [12, 13]. With increasing compressive loading, the average longitudinal elastic strain $e_{22}$ becomes more negative, while the average elastic transverse strains $e_{11}$ (perpendicular to the direction of the applied load) become more positive, with a slope of 475 GPa, much larger than the apparent modulus. Thus, the average state of stress of the alumina phase upon compressive loading seems to be close to uniaxial compressive (with $e_{11}$=-ν $e_{22}$, where ν is Poisson's ratio). Finally, residual strains are present under zero applied stress, as expected from the thermal expansion mismatch between the phases. These strains are tensile in the longitudinal directions and compressive in the transverse direction.

Similar to plots shown for $Al_2O_3$ (hkl) planes, a plot for $ZrO_2$ (101) plane is presented in Figure 3b. Upon cyclical loading, the apparent elastic modulus of the zirconia phase ($E_{app}$=175 GPa) was lower than the elastic modulus of pure partially stabilized $ZrO_2$ (E=205 GPa). While load sharing occurs in a similar manner as for the alumina phase, the maximum longitudinal

strain in the zirconia phase is about 60% higher than in the alumina phase. Like for the $Al_2O_3$ (113) reflection, the average state of stress of the zirconia phase is close to uniaxial compressive, residual strains are present under zero applied stress and no large-scale damage was evident during cyclical loading.

A second face-centered-cubic symmetry composite was compression tested to failure (ca. 250 MPa) while spatially resolved diffraction measurements were collected. This composite exhibited a density of 3.35 g/cm$^3$, corresponding to a 99.99% pure Al volume fraction of 48.9%. Like the previous composite, plots of the applied stress vs. elastic lattice strain were created for several $Al_2O_3$ and $ZrO_2$ (hkl) planes. One such plot for the $Al_2O_3$ (113) plane, which is representative of typical $Al_2O_3$ (hkl) planes, is presented in Figure 4 along with two rule-of-mixture models.

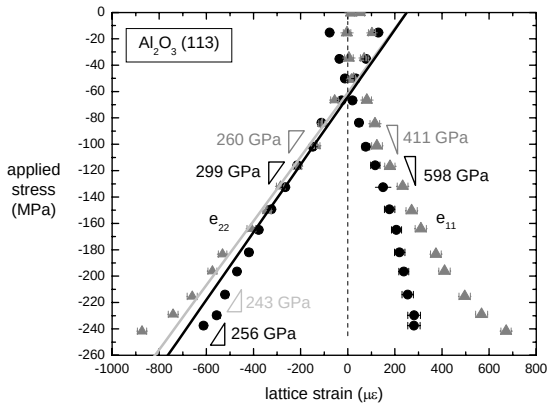


Figure 4. Applied stress vs. lattice strain for Al/$Al_2O_3$ composites with face-centered-cubic symmetry, using $Al_2O_3$ (113) reflection, upon cyclical loading. The values of the two rule-of-mixture models are shown at the bottom of the figure.

Similar to the average strain plot in Figure 3a, load transfer is evident between the alumina and aluminum phases. However, in this case, load transfer varies with position. In matrix-dominated regions where only the alumina "hairpins" (horizontal struts) are present, the slopes ($E_{app}$=260 and 411 GPa for $e_{22}$ and $e_{11}$, respectively) are lower than in the reinforcement-dominated regions (along a row of struts and columns) where the slopes are 299 and 598 GPa, respectively. Additionally, plasticity in the matrix dominated region is inferred beyond 200 MPa from the deviation of the elastic line, while plasticity is not observed in the reinforcement dominated region.

Two models based on the rule-of-mixture provided apparent elastic moduli for the alumina phase ($E_{app}$=243 GPa and $E_{app}$=256 GPa for $e_{22}$) within the error of experimental data for the face-centered-cubic symmetry composites, as shown in Figure 4 [14]. The first model assumes that all alumina (in both struts and columns) is present as longitudinal fibers within the aluminum matrix, from which a longitudinal "equi-strain" composite modulus and the strain in the alumina phase can be calculated. The second model considers two regions: (a) alumina within columns, and (b) a mixture of alumina horizontal struts and aluminum matrix. The latter region is modeled as an "equi-stress" composite which is put in parallel with the former region in an "equi-strain" composite. The total alumina strain is then obtained by a volume averaging of the strains in the alumina columns and struts.

Similar results were obtained for simple-cubic symmetry composites with the major difference being that the simple-cubic symmetry has higher strength than the face-centered-cubic symmetry composite due to the inherent strength in having vertical columns rather than zigzagging columns as illustrated in Figure 1 and previously noted [8].

## CONCLUSIONS

Interpenetrating $Al_2O_3$-Al composites were produced by liquid-metal infiltration of 3-D periodic $Al_2O_3$ preforms with spanning elements that were fabricated by robotic deposition. X-ray phase-enhanced images were collected from ceramic preforms and pre- and post-compression testing composites of both simple-cubic and face-centered-cubic symmetry providing information on localized damage in the composite. These composites were compressed uniaxially while subjected to x-ray diffraction measurements allowing for measurement of load transfer occurring between the metal and ceramic phase. As illustrated for one preform geometry, load transfer can be predicted in the elastic regime with simple rule-of-mixture models.

## ACKNOWLEDGMENTS

The author would like to thank Ranjeet Rao and Professor Jennifer A. Lewis at the University of Illinois at Urbana-Champaign ($Al_2O_3$ preforms), and Dr. Mark Beno and Chuck Kurtz at the APS (BESSRC-CAT) at ANL (diffraction setup). Use of the APS was supported by the U.S. Department of Energy, Office of Science, Office of Basic Energy Science, under contract number W-31-109-Eng-38.

## REFERENCES

[1] A. Zimmermann, M. Hoffman, T. Emmel, D. Gross, J. Rodel, Acta Materialia 49 (2001) 3177-3187.
[2] K. G. Ewsuk, S. J. Glass, R. E. Loehman, A. P. Tomsia, W. G. Fahrenholtz, Metallurgical and Materials Transactions A 27 (1996) 2122.
[3] W. Liu, U. Koster, Materials Science and Engineering A 210 (1996) 1-7.
[4] J. E. Smay, J. Cesarano, J. A. Lewis, Langmuir 18 (2002) 5429-5437.
[5] J. E. Smay, G. M. Gratson, R. F. Shepherd, J. Cesarano, J. A. Lewis, Advanced Materials 14 (2002) 1279-1283.
[6] J. Cesarano, P. Calvert, US Patent, 2000.
[7] C. San Marchi, M. Kouzeli, R. Rao, J. A. Lewis, D. C. Dunand, Scripta Materialia 49 (2003) 861-866.
[8] M. L. Young, J. D. Almer, U. Lienert, D. R. Haeffner, R. Rao, J. A. Lewis, D. C. Dunand, Materials Science and Technology, Chicago, IL, 2003.
[9] A. Mortensen, *Comprehensive Composite Materials*, Elsevier, New York, 2000.
[10] P. Cloetens, R. Barrett, J. Baruchel, J. P. Guigay, M. Schlenker, Journal of Physics D: Applied Physics 29 (1996) 133-146.
[11] A. Wanner, D. C. Dunand, Metallurgical and Materials Transactions A 31 (2000) 2949-2962.
[12] D. C. Dunand, D. Mari, M. A. M. Bourke, J. A. Roberts, Metallurgical and Materials Transactions A 27 (1996) 2820-2836.
[13] A. J. Allen, M. A. M. Bourke, S. Dawes, M. T. Hutchings, P. J. Withers, Acta Metallurgica et Materialia 40 (1992) 2361-2373.
[14] T. H. Courtney, *Mechanical Behavior of Materials*, McGraw Hill, 2000.